

Photonic crystal slot-microcavity circuit implemented in silicon-on-insulator: High Q operation in solvent without undercutting

S. Hamed Mirsadeghi, Ellen Schelew, and Jeff F. Young

Citation: *Appl. Phys. Lett.* **102**, 131115 (2013); doi: 10.1063/1.4799963

View online: <http://dx.doi.org/10.1063/1.4799963>

View Table of Contents: <http://apl.aip.org/resource/1/APPLAB/v102/i13>

Published by the [American Institute of Physics](http://www.aip.org).

Additional information on *Appl. Phys. Lett.*

Journal Homepage: <http://apl.aip.org/>

Journal Information: http://apl.aip.org/about/about_the_journal

Top downloads: http://apl.aip.org/features/most_downloaded

Information for Authors: <http://apl.aip.org/authors>

ADVERTISEMENT

a sampling of our products		for surface and materials science	www. rbdinstruments .com	celebrating over 20 years of innovation
 deposition tools	 desorption systems	 sputter ion sources	 viewports	 usb picoammeters

Photonic crystal slot-microcavity circuit implemented in silicon-on-insulator: High Q operation in solvent without undercutting

S. Hamed Mirsadeghi,^{a)} Ellen Schelew,^{b)} and Jeff F. Young^{c)}

Department of Physics and Astronomy, Advanced Materials and Processing Engineering Laboratory (AMPEL), University of British Columbia, Vancouver, British Columbia V6T 1Z1, Canada

(Received 13 December 2012; accepted 22 March 2013; published online 5 April 2013)

We report the fabrication and characterization of a silicon-based photonic integrated circuit consisting of a photonic crystal slot-cavity, waveguides, and grating couplers, designed as a robust, easy-to-use device for enhancing light-matter interactions at a precise location inside a fluidic medium, while minimizing fabrication complexity. Measured Q values in excess of 7500 for circuits immersed in hexane and operating near $1.5\ \mu\text{m}$ are obtained, in good agreement with simulations. The detection limit for changes in solvent refractive index unit (RIU) for these structures, which have not been optimized, is 2.3×10^{-5} RIU. © 2013 American Institute of Physics.

[<http://dx.doi.org/10.1063/1.4799963>]

Strong light-matter interaction is critical for both fundamental studies and applications including nonlinear optics, cavity quantum electrodynamics (QED), optical sensing, and optical trapping. Optical resonators such as Fabry-Perot cavities,¹ microspheres,² silicon and silica whispering gallery type resonators,³ and photonic crystal (PC) nanocavities^{4,5} are known to enable such strong interaction by both spectrally and spatially confining light. These structures are characterized by three key parameters, quality factor (Q), which is a measure of losses in a cavity, mode volume (V), and the overall transmission (T) of the excitation source. High Q , small V cavities can be used to increase spontaneous emission rates,⁶ optical nonlinear responses,⁷ and optomechanical coupling;⁸ to decrease the optical power required to achieve “strong coupling” in cavity QED,^{9,10} optically trap nanoparticles,^{11,12} and push the limits of molecular detection;¹³ and to decrease the electrical power needed to drive optical modulators¹⁴ and lasers.¹⁵

Of the various cavity-based approaches, PC microcavities^{4,5} are attractive because of the *combination* of high Q factors *and* low mode volumes that can be achieved, their design flexibility, and the ease of integrating them in planar lightwave circuits (PLCs). The present work focusses on silicon-on-insulator (SOI) PLCs, and exploits the design flexibility of PCs to integrate high- Q , low mode-volume microcavities, wherein the mode energy resides almost entirely in the background dielectric (vacuum or a solvent), with more conventional SOI-based grating couplers, and silicon wire-waveguides, where the field is predominantly in the silicon. Such structures are of interest for applications where one wants to enhance the interaction of circuit-bound photons with matter that cannot be embedded within the silicon. Examples include optical sensing, where small amounts of some material in solution are detected due to its effect on changing the refractive index of the pure solvent and trapping of small, nanoscale objects suspended in solution, using optical forces.

Almeida *et al.*¹⁶ developed “slot-waveguide” structures that support propagating modes in silicon-based waveguides wherein most of the mode profiles are concentrated in the air/solvent gap between two silicon ridges. These have been used extensively in the sensor community.^{17,18} Robinson *et al.*¹⁹ theoretically showed that if such a slot waveguide was surrounded by a one dimensional PC on either end, a fully three dimensional (3D) localized mode could be trapped in a volume less than a tenth of a cubic half (free space) wavelength. This design assumed a slot width of only 20 nm. Yamamoto *et al.*⁵ used a two dimensional (2D) PC to create a similarly small mode volume cavity in a wider slot waveguide. In this design, which is easier to fabricate, the cavity was defined by locally modifying just a few of the holes in the PC, nearest to the waveguide. Di Falco *et al.*²⁰ demonstrated high Q values and strong sensitivity of resonant frequencies to the background refractive index in slot cavities defined by varying the pitch of the surrounding PC along the slot waveguide axis. These, as well as subsequent¹⁰ high Q PC based slot cavities, are based on “free-standing” structures where the underlying cladding layer is removed after the PC structures are etched into the silicon. They also required butt-coupling of the excitation source to the waveguide.

Here, we incorporate slot cavities in full SOI photonic circuits that include input/output grating couplers, single mode silicon ridge waveguides, and one dimensional (1D) PC coupling waveguides. The cavities are designed to support high Q modes in solution without having to remove the silicon dioxide layer beneath the cavities. The circuit layout is shown in various levels in detail in Fig. 1. Two 2D photonic crystal grating couplers²¹ of hole radius 250 nm separated by $680\ \mu\text{m}$ are used to launch light from a tunable laser diode, via parabolic tapered waveguides, into and out of single mode silicon channel waveguides that connect to the photonic crystal cavity region. The background PC region comprises a hexagonal array of circular holes separated by 490 nm, and with hole radius of $r = 160\ \text{nm}$. Various “defects” are introduced into this background PC, in order to excite a 3D localized mode in the centre of the PC. All data and simulations in this manuscript correspond to samples with a 220 nm thick silicon layer on top of a

^{a)}Electronic mail: hamedms@phas.ubc.ca

^{b)}Electronic mail: eschelew@phas.ubc.ca

^{c)}Electronic mail: young@phas.ubc.ca

3 μm thick buried oxide layer that robustly supports all circuit elements.

The single mode channel waveguides of width 450 nm are connected via a short impedance matching region^{22,23} to “W1” photonic crystal waveguides that simply omit a row of holes from the background PC. Slots of widths $s = 70$ nm, 90 nm, or 110 nm run horizontally, through the middle of the PC, forming a distinct 1D waveguide that intersects the W1 waveguides at 60° . The light in the W1 waveguides propagates primarily in the silicon, while the slot waveguides confine the light primarily in the air or solvent gap. Fig. 1(c) shows how the two different waveguide types are connected, via a single “coupling hole” with radius (r_c) that varies from chip to chip. This geometry, though not yet optimized, allows independent access to the slot waveguide from the ends, which may be advantageous for some applications.

When the position of the holes adjacent to the slot waveguide between the two W1 waveguides are intentionally shifted away from the slot, a 3D localized mode is drawn out of the slot waveguide continuum,⁵ and it is this 3D localized mode that is exploited in this circuit design. For all of our samples, the shifts of the holes are as shown in Fig. 1(d).

The samples were fabricated²⁴ using a 100 keV JEOL JBX-6300FS electron beam writing system and ZEP-520 A resist (Nippon-Zeon Co. Ltd.), which served as the etch

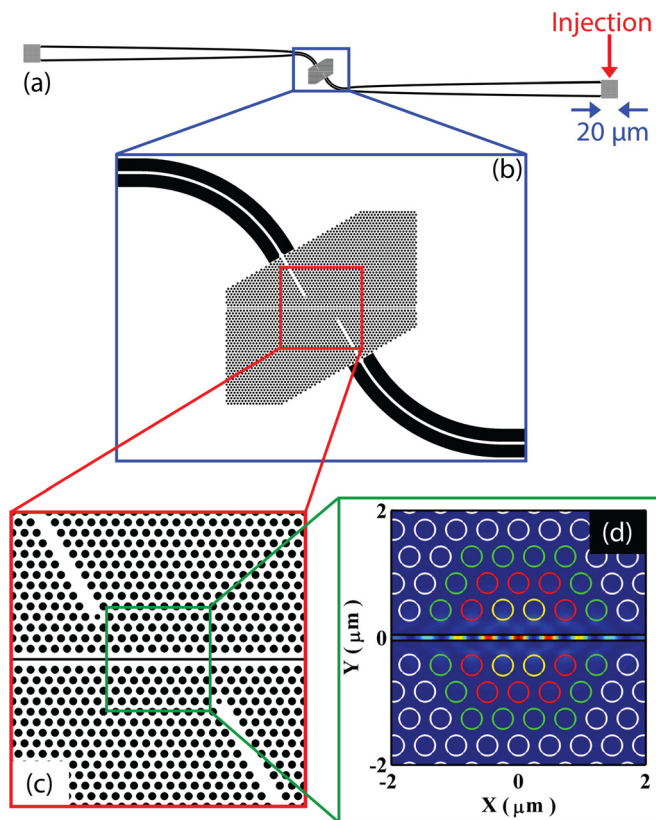


FIG. 1. (a)–(c) Layout of a slot-cavity with input/output grating couplers, tapered and ridge waveguides. The excitation laser injection location is labeled. The two smaller “coupling holes” at the end of PC waveguides are visible in (c). (d) The electric field intensity distribution of the slot-cavity from 3D FDTD simulations overlapped with the cavity design. To make the defects in the PC lattice, yellow, red, and green holes are shifted by 12, 8, and 4 nm, respectively. Note that the field in the cavity is almost entirely polarized in the y direction.

mask. Etching was done using an Oxford PlasmaLab System 100 with chlorine gas. The complete circuit requires only one lithography step and one etch step.

Fig. 1(d) also shows the electric field intensity distribution in the vicinity of the slot-cavity mode, calculated using finite difference time domain (FDTD) software.²⁵ A transverse electric (TE)-polarized mode with well-defined power in the input silicon channel waveguide is launched towards the cavity region, and the corresponding power in the output silicon channel waveguide is calculated using a 2D frequency-domain power monitor, from which the simulated transmission is obtained, as shown in Fig. 2(a). These simulations correspond to the device parameters of sample S2 in Table I, and assume the holes and top half space are filled with hexane ($n = 1.365$). Hexane is of interest because it is our preferred solvent for suspending colloidal Pb-based quantum dots that can be tuned in resonance with these cavities.

Fig. 2(a) shows the experimentally measured transmission spectrum through sample S2, in hexane, on an absolute scale (left curve). These data were obtained by focussing a tunable continuous wave (CW) laser to a 10 μm diameter on the input grating coupler (“Injection” label in Fig. 1(a)), and monitoring the power emitted from the corresponding output grating coupler. To make a correspondence with simulated transmission from ridge waveguide to ridge waveguide, these cavity transmission spectra were normalized by the transmission measured through identical reference samples where the entire PC region in Fig. 1(b) is replaced by a simple continuation of the ridge waveguide.

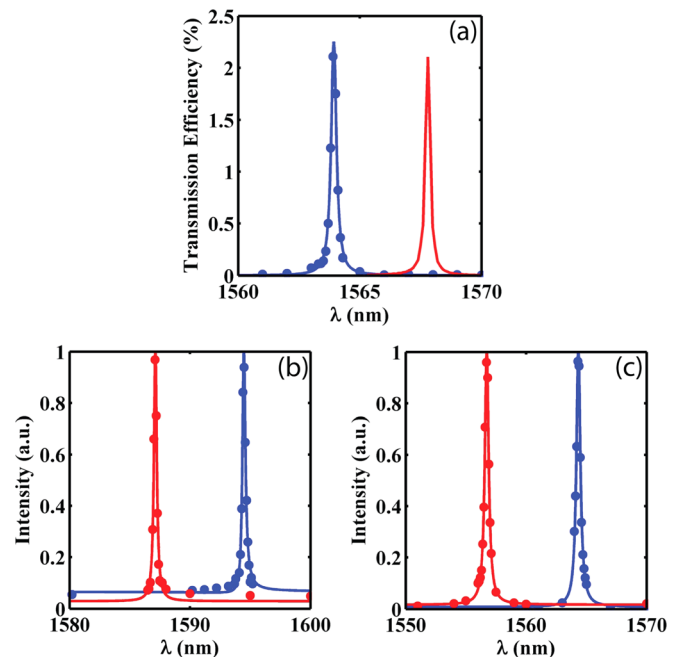


FIG. 2. (a) Resonant transmission spectra from input to output ridge waveguides through slot-cavity for sample S2 in Table I. The simulation curve is red (right curve) and the experimental data points fitted with a Fano lineshape are plotted in blue (left curve). (b) and (c) Resonant transmission spectra for two different devices in hexane (blue, on the right) and acetone (red, on the left): (b) $r = 160$ nm, $s = 70$ nm, $r_c = 80$ nm, $Q_{\text{hexane}} = 5450$, $Q_{\text{acetone}} = 5700$, (c) $r = 160$ nm, $s = 90$ nm, $r_c = 80$ nm, $Q_{\text{hexane}} = 3980$, $Q_{\text{acetone}} = 4100$.

TABLE I. Summary of the results from simulations and transmission measurements on 5 different devices.

Sample ^a	s (nm)	r_c (nm)	Simulation			Experiment		
			λ (nm)	Q	T (%) ^b	λ (nm)	Q	T (%) ^b
S1	90	80	1567.8	5640	4.8	1564.3	3800	3.1±0.4
S2	90	110	1567.8	7390	2.1	1563.9	6100	2.3±0.3
S3	90	140	1567.8	8480	0.49	1564.8	4400	0.29±0.08
S4	70	110	1596	8900	...	1595.4	7650	...
S5	110	110	1535.4	4720	...	1545.2	4400	...

^aFor all devices in this table, $r = 160$ nm.

^bThese values are the transmission between input and output ridge waveguides at the resonance of the cavities.

Table I summarizes the measured and simulated parameters for 5 different samples (absolute transmission data only for 3 of the 5). Samples S1, S2, and S3 differ only in the radius of the “coupling hole.” Samples S1 and S2 both yield good agreement with the simulations, while all parameters for sample S3 are noticeably different, indicating a fabrication error. Samples S2, S4, and S5 differ only in the width of the slot, and the predicted shift and change in Q value are in good agreement between experiment and simulation.

These Q values are higher than those reported for cavities operating in solvents in Refs. 11, 20, and 26 despite not having removed the silicon dioxide undercladding. Simulations suggest that by undercutting these cavities, the *intrinsic* (i.e., stand-alone, unloaded) Q value of the cavity in hexane should increase from 10×10^3 to 25×10^3 as compared to the hexane-over-SiO₂ structure studied here. The transmission values are limited partially by the fact that the W1 photonic crystal waveguide modes turned out to be above the light line in these samples (a total propagation loss of ~ 1.5 dB), and because the single-variable-hole coupler between the W1 waveguide and the slot waveguide causes excess scattering.

To illustrate the impact of working with a cavity mode localized in the slot, Figs. 2(b) and 2(c) show the spectra for two samples measured in hexane and acetone ($n = 1.346$). All modes shift by ~ 7 nm, consistent with simulations. The largest shift in nm per unit variation in refractive index (sensitivity) is 370 nm RIU^{-1} , for sample S2. This is less than that reported for some samples in Ref. 20 because their structures are undercut, and because they have larger slot widths. Using the definition of the detection limit (DL) in Ref. 27, these Q values, sensitivity, and our signal to noise ratio (SNR) of 33 dB with 0.8 mW excitation power, the DL of these structures is estimated to be 2.3×10^{-5} RIU. This is comparable to other photonic crystal sensors^{20,26,28,29} based on undercut cavities. Despite the fact that the Q values reported in Table I are lower than Refs. 30 and 31, these devices have larger sensitivity as a result of shifting the field maximum from the slab into the fluid.

In conclusion, we have reported the design, fabrication, and characterization of a silicon-based photonic integrated circuit consisting of a photonic crystal slot-cavity, waveguides, and grating couplers, operating at telecommunication wavelengths in a fluidic medium. The structure was designed to offer a robust means to enhance electric field intensity and hence light-matter interactions at a precise location inside a

fluidic medium, while minimizing fabrication complexity and maximizing ease-of-use. Both 3D FDTD simulations and transmission measurements demonstrate that such circuits, fabricated in a single lithography/single etch process without having to undercut the cavity, exhibit Q factors >7500 and mode volumes of $V \sim 0.086(\frac{\lambda}{n})^3$, with resonant transmission $T \sim 3\%$, when operated in hexane. These unoptimized structures have a detection limit for refractive index change of $\sim 2 \times 10^{-5}$ RIU. Their performance could be improved by (i) modifying the sizes of the holes that line the W1 waveguide and the junction between it and the slot waveguide, to reduce losses and improve the SNR, (ii) by reducing the hole-shifts that define the slot cavity, thus enhancing the unloaded Q , and (iii) by using a different cladding layer thickness to increase the grating coupling efficiency.²¹

The authors acknowledge support from the Natural Science and Engineering Research Council (Canada), the Canadian Institute for Advanced Research, and Lumerical Solutions, Inc.,²⁵ We thank Dr. Lukas Chrostowski, Richard Bojko, and University of British Columbia AMPEL Nanofabrication Facility. Part of this work was conducted at the University of Washington Microfabrication/Nanotechnology User Facility, a member of the NSF National Nanotechnology Infrastructure Network. Computational support was provided by Lumerical Solutions, Inc.,²⁵ and grid-enabled computational resources were provided by WestGrid.

- ¹K. J. Vahala, *Nature (London)* **424**, 839–846 (2003).
- ²I. S. Grudin, A. B. Matsko, and L. Maleki, *Opt. Express* **15**, 3390–3395 (2007).
- ³D. K. Armani, T. J. Kippenberg, S. M. Spillane, and K. J. Vahala, *Nature (London)* **421**, 925–928 (2003).
- ⁴S. Noda, M. Fujita, and T. Asano, *Nat. Photonics* **1**, 449–458 (2007).
- ⁵T. Yamamoto, M. Notomi, H. Taniyama, E. Kuramochi, Y. Yoshikawa, Y. Torii, and T. Kuga, *Opt. Express* **16**, 13809–13817 (2008).
- ⁶A. G. Pattantyus-Abraham, H. Qiao, J. Shan, K. A. Abel, T.-S. Wang, F. C. J. M. van Veggel, and J. F. Young, *Nano Lett.* **9**, 2849–2854 (2009).
- ⁷I. B. Burgess, Y. Zhang, M. W. McCutcheon, A. W. Rodriguez, J. Bravo-Abad, S. G. Johnson, and M. Loncar, *Opt. Express* **17**, 20099–20108 (2009).
- ⁸A. H. Safavi-Naeini, T. P. M. Alegre, M. Winger, and O. Painter, *Appl. Phys. Lett.* **97**, 181106 (2010).
- ⁹K. Hennessy, A. Badolato, M. Winger, D. Gerace, M. Atature, S. Gulde, S. Falt, E. L. Hu, and A. Imamoglu, *Nature (London)* **445**, 896–899 (2007).
- ¹⁰J. Gao, J. F. McMillan, M.-C. Wu, J. Zheng, S. Assefa, and C. W. Wong, *Appl. Phys. Lett.* **96**, 051123 (2010).
- ¹¹C. Renaud, J. Dellinger, B. Cluzel, T. Honegger, D. Peyrade, E. Picard, F. de Fornel, and E. Hadji, *Appl. Phys. Lett.* **100**, 101103 (2012).
- ¹²P. T. Lin and P. T. Lee, *Opt. Express* **20**, 3192–3199 (2012).
- ¹³Y. Liu and H. W. M. Salemink, *Opt. Express* **20**, 19912–19920 (2012).
- ¹⁴J. D. Ryckman, V. Diez-Blanco, J. Nag, R. E. Marvel, B. K. Choi, R. F. Haglund, and S. M. Weiss, *Opt. Express* **20**, 13215–13225 (2012).
- ¹⁵S. Matsuo, A. Shinya, T. Kakitsuka, K. Nozaki, T. Segawa, T. Sato, Y. Kawaguchi, and M. Notomi, *Nat. Photonics* **4**, 648–654 (2010).
- ¹⁶V. R. Almeida, Q. Xu, C. A. Barrios, and M. Lipson, *Opt. Lett.* **29**, 1209–1211 (2004).
- ¹⁷F. Dell’Olio and V. M. Passaro, *Opt. Express* **15**, 4977–4993 (2007).
- ¹⁸C. A. Barrios, K. B. Gylfason, B. Sanchez, A. Griol, H. Sohlström, M. Holgado, and R. Casquel, *Opt. Lett.* **32**, 3080–3082 (2007).
- ¹⁹J. T. Robinson, C. Manolatu, L. Chen, and M. Lipson, *Phys. Rev. Lett.* **95**, 143901 (2005).
- ²⁰A. Di Falco, L. O’Faolain, and T. F. Krauss, *Appl. Phys. Lett.* **94**, 063503-3 (2009).
- ²¹E. Schelew, G. Rieger, and J. Young, *J. Lightwave Technol.* **31**, 239–248 (2013).

- ²²E. Miyai and S. Noda, *J. Opt. Soc. Am. B* **21**, 67–72 (2004).
- ²³M. G. Banaee, A. G. Pattantyus-Abraham, M. W. McCutcheon, G. W. Rieger, and J. F. Young, *Appl. Phys. Lett.* **90**, 193106-3 (2007).
- ²⁴R. J. Bojko, J. Li, L. He, T. Baehr-Jones, M. Hochberg, and Y. Aida, *J. Vac. Sci. Technol. B* **29**, 06F309-6 (2011).
- ²⁵Lumerical Solutions, Inc. <http://www.lumerical.com/tcad-products/fdtd/>.
- ²⁶M. Scullion, A. Di Falco, and T. Krauss, *Biosens. Bioelectron.* **27**, 101–105 (2011).
- ²⁷I. M. White and X. Fan, *Opt. Express* **16**, 1020–1028 (2008).
- ²⁸B. Wang, M. A. Dunder, R. Notzel, F. Karouta, S. He, and R. W. van der Heijden, *Appl. Phys. Lett.* **97**, 151105-3 (2010).
- ²⁹E. Chow, A. Grot, L. W. Mirkarimi, M. Sigalas, and G. Girolami, *Opt. Lett.* **29**, 1093–1095 (2004).
- ³⁰W. C. Lai, S. Chakravarty, Y. Zou, and R. T. Chen, *Opt. Lett.* **37**, 1208–1210 (2012).
- ³¹K. Yao and Y. Shi, *Opt. Express* **20**, 27039–27044 (2012).